ECONOMIC ANALYSIS OF ARTIFICIALLY ROUGHENED SOLAR AIR HEATER WITH V-SHAPED RIBS

Rahul Bahuguna*
Department of Thermal Engineering, Faculty of Technology
Veer Madho Singh Bhandari Uttarakhand Technical University
Dehradun, Uttarakhand, 248007, India, rahul.bahuguna25@gmail.com
https://orcid.org/0000-0002-9058-7460

Sunil Chamoli
Department of Mechanical Engineering
Govind Ballabh Pant Institute of Engineering & Technology
Pauri Garhwal, Uttarakhand, 246194, India
https://orcid.org/0000-0002-4031-9775

Yogesh Barthwal
Department of Mechanical Engineering
Govind Ballabh Pant Institute of Engineering & Technology
Pauri Garhwal, Uttarakhand, 246194, India
https://orcid.org/0000-0003-0584-0722

Sumit Rana
Department of Mechanical Engineering
Govind Ballabh Pant Institute of Engineering & Technology
Pauri Garhwal, Uttarakhand, 246194, India
https://orcid.org/0000-0003-3753-3997

Ashutosh Gupta
Department of Mechanical Engineering
Govind Ballabh Pant Institute of Engineering & Technology
Pauri Garhwal, Uttarakhand, 246194, India
https://orcid.org/0000-0003-3109-1884

Vijay Singh Bisht
Department of Thermal Engineering, Faculty of Technology
Veer Madho Singh Bhandari Uttarakhand Technical University
Dehradun, Uttarakhand, 248007, India
https://orcid.org/0000-0002-7728-8896

Article history: Received 17 March 2022, Received in revised form 20 April 2022, Accepted 4 May 2022, Available online 4 May 2022

Highlight

Life cycle savings as performance evaluation criterion is used to evaluate the economic performance of solar air heater.

Abstract

Due to the minimal transfer of heat from absorber plate to moving air in the duct, solar air heaters have low performance. One of the procedures to augment the heat transfer by substantial amount is by utilizing artificial roughness, by which the performance can be improved considerably. In this study, an economic investigation of solar air heater embedded with artificial roughness is accomplished numerically employing v-shaped roughness, with the objective of optimising life cycle solar savings. The non-dimensional parameters of roughness, namely, angle of attack (α), roughness pitch (p/e) and roughness height (e/D_h) are examined

by varying temperature rise over the solar air heater (*ΔT*) and solar radiations (*I*) for different economic parameters values i.e., cost of collector, cost of roughness elements, and cost of conventional fuel.

Keywords
solar air heater; heat transfer; artificial roughness; economic analysis; life cycle savings.

Introduction

Solar air heater (SAH) is the most used heat exchanger which is used to convert the solar radiations coming onto the earth's surface into heat. This heat is then transferred to the flowing air below the absorber plate of SAH. As the thermal conductivity value of air is less, the transfer of heat among the air and the absorber plate is ineffective. Owing to this, numerous alterations to the SAH are considered by various researchers to elevate the transfer of heat between the air and absorber plate. One among the most successful approach to augment the transfer of heat in SAHs is by using artificial roughness in the form of ribs below the absorber plate. The artificial rib roughness introduces the disturbance in the flow by mixing and promoting turbulence in fluid flow, thereby breaking the viscous sublayer at absorber plate's surface, and induces secondary flows, which augments the transfer of heat and accumulate less rise in pumping power.

Prasad and Mullick [1] incorporated artificial roughness in SAH to elevate the transfer of heat initially. They used protruding wires for improving the plate efficiency factor of SAHs from 0.63 to 0.72, corresponding to an enhancement in the performance of 14%. Momin et al. [2] examined the impact of v-shaped roughness in a duct of the SAH, and recorded that for v rib, the utmost elevation in Nusselt number (*Nu*) and friction factor (*f*) was 2.30 and 2.83 times concerning smooth duct, respectively. Hans et al. [3] used multiple v-rib as roughness in SAH duct and reported a maximum enhancement in *Nu* and *f* of 6 and 5 times concerning smooth duct. Chamoli and Thakur [4] used v-shaped baffles with perforation and reported enhancement in *Nu* and *f* of 2.2 and 5.5 times concerning smooth duct. Gawande et al. [5] incorporated chamfered square ribs and reported a maximum thermal-hydraulic performance of 2.047. Maithani and Saini [6] applied v ribs with gaps at symmetry and recorded an utmost elevation in *Nu* and *f* of 3.6 and 3.67 times concerning smooth tube. Nadda et al. [7] employed multiple arc protrusions obstacles in a jet impingement SAH and reported that the optimal improvement is achieved at a width ratio of five, angle of attack of 55°. Bisht et al. [8] compared different roughness geometries based on their thermal and exergetic performance and gave a comprehensive review of the roughness geometries. Singh and Singh [9] incorporated square cross sectioned transverse ribs as roughness and reported the highest thermo-hydraulic performance factor of 1.43 at a pitch ratio value of 10. Chamoli et al. [10] used winglet vortex generators as roughness and reported thermal enhancement factor ranging from 1.72 to 2.20. Maithani et al. [11] incorporated spherical shaped turbulence promoters and reported a maximum value of enhancement factor of 2.98. Similar strategies to raise the heat transfer using different novel inserts to augment thermal performance of heat exchangers was reported by various researchers like Bahuguna et al. [12], Paneliya et al. [13], Bahuguna et al. [14], Kumar and Chandra. [15]. Bisht et al. [16] employed v ribs in conjunction with perforated baffles of the shape of v and recorded that utmost *Nu* and thermal efficiency comes at an open area ratio of 12%. Choi and Choi [17] employed transverse triangular block type ribs in SAH and reported an utmost augmentation in *Nu* of 3.37 over smooth duct. Ghritlahre et al. [18] studied the works related to energy and exergy analysis of distinct types of solar air heaters and reported that the energetic and exergetic efficiencies of distinct types of SAHs varied from 2.05% to 82% and 0.01% to 60.97%, respectively. Singh et al. [19] used kite-shaped ribs in SAH and reported an utmost augmentation in *Nu* of 4.8 times than that of a smooth tube, and highest thermohydraulic performance of 2.9. Azadani and Gharouni [20] employed cylindrical shape roughness and reported a thermohydraulic performance of 1.20 for best parameters of roughness. Haldar et al. [21] numerically investigated artificial wavy ribs in SAH and reported the optimum thermohydraulic performance parameter of 1.96. Likewise, a number of investigators used different orientations of ribs to enhance *Nu* with a minimal increase in *f*.

According to the author's information, the thermal performance of SAH along with its economic analysis have never been reported together, therefore there is a need to assess the value of solar thermal systems by considering the economic aspects to check their feasibility. Once the thermal performance of SAH is evaluated, the methods for making economic evaluations are required. Based on life cycle solar savings, an economic analysis of an artificially roughened SAH utilising v-shaped ribs as roughness was conducted in this study. The impact of roughness parameters, namely, e/D_h, p/e, and α, on life cycle savings (*LCS*) of SAH for various values of collector cost factors, with respect to design parameter i.e., insolation (*I*) and temperature rise parameter ($\Delta T/I$) have been studied. This research is conducted in Dehradun, which is the capital of Indian State Uttarakhand where temperature varies from around 10°C to 40°C in a year, with mostly sunny all around the year making it appropriate to use solar energy utilization system. Also, as this research work is based on financial

aspect of solar air heater, hence it is imperative to know the conventional solar air heater cost which is around $1/Watt, and if artificial roughness is applied to it than the cost may increase by around 25%.

System Model

For this investigation, below the SAH's absorber plate a continuous v-down ribs are applied using a wire as roughness elements. The parameters of roughness i.e., e/D_h, p/e, and α have been varied. The useful heat gain (Q_u), is determined from the following relationship for SAH:

(1) $$Q_u = F_R A_p\{I(\tau\alpha) - U_l(T_o - T_i)\}$$

where, A_p is surface area of absorber plate, ($\tau\alpha$) is transmittance-absorptance product U_l is Overall heat loss coefficient, T_o and T_i is outlet and inlet temperature of air, F_R is heat removal factor given by,

(2) $$F_R = \frac{GC_p}{U_l}\left\{exp\left(\frac{F'U_l}{GC_p}\right) - 1\right\}$$

where, G is mass velocity of air, C_p is specific heat of air, F' is collector efficiency factor.
The roughness geometry of repeated continuous v-down ribs analysed in this work is shown in Figure 1.

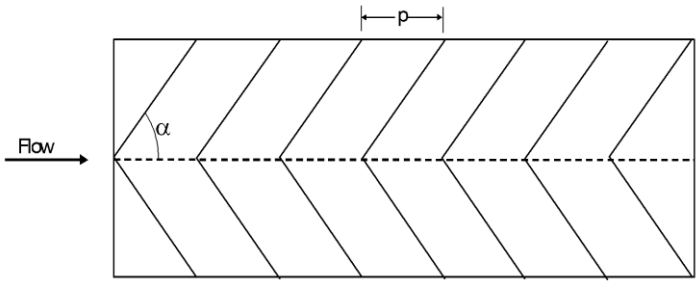

Figure 1. Continuous v-down rib geometry analysed in present work.

It is seen from the geometry of multiple v-shape rib roughness investigated by Hans et al. [3], that if the width of single v-rib (w) is same as width of plate i.e. (W/w) = 1, the roughness geometry so obtained will be identical with the one, which is been considered in the present study (Figure 1). So, by using the value of W/w as 1 in the correlations of Nu and f given by Hans et al. [3], the modified correlations of Nu and f are presented in Eqs. 3 and 4, respectively, and are used in the present study:

(3) $$Nu = 0.0000335(Re)^{0.92}\left(\frac{e}{D_h}\right)^{0.77}\left(\frac{p}{e}\right)^{8.54}\left(\frac{\propto}{90}\right)^{-0.49} exp\left\{-0.61\left(ln\frac{\propto}{90}\right)^2\right\} exp\left\{-2.0407\left(ln\frac{p}{e}\right)^2\right\}$$

(4) $$f = 0.000447(Re)^{-0.3188}\left(\frac{e}{D_h}\right)^{0.73}\left(\frac{p}{e}\right)^{8.9}\left(\frac{\propto}{90}\right)^{-0.39} exp\left\{-0.52\left(ln\frac{\propto}{90}\right)^2\right\} exp\left\{-2.133\left(ln\frac{p}{e}\right)^2\right\}$$

The top loss coefficient (U_t) in the present study is found by using the correlation reported by Malhotra et al.[22] as:

(5) $$U_t = \left[\frac{N}{\left(\frac{C}{T_m}\right)\left(\frac{T_m - T_a}{N + f_e}\right)^{0.252}} + \frac{1}{h_w}\right]^{-1} + \left[\frac{\sigma(T_m^2 + T_a^2)(T_m + T_a)}{\frac{1}{\varepsilon_p + 0.0425N(1 - \varepsilon_p)} + \frac{2N + f_e - 1}{\varepsilon_g} - N}\right]$$

where, N is number of glass covers in SAH, C is an empirical factor (= $620(1-0.000051\beta^2)$ for $0°<\beta<70°$ and for $70°<\beta<90°$ use $\beta = 70°$, β is tilt angle of SAH), T_m is mean plate temperature, T_a is ambient temperature, f_e is an empirical factor (= $(1+0.089h_w - 0.1166h_w\epsilon_p)(1+0.07866N)$), h_w is wind heat transfer coefficient (=$5.7+3.8V_w$, V_w is wind speed), σ is the Stefan Boltzmann constant, ϵ_p is emissivity of absorber plate, ϵ_g is emissivity of glass cover. The operating and system parameters employed for the present investigation are presented in Table 1.

Table 1. Specification and range of parameters of the investigation.

Fixed Parameters	**Values**	**Variable Parameters**	**Range of parameters**
L	2	e/D_h	0.020-0.044
W	1	p/e	6-12
H	0.025	α	30-75
N	1	$\Delta T/I$	0.002-0.025
$(\tau\alpha)$	0.80	I	1000
T_a	300	C_C	1000-20000
f_l	0.8	C_R	2-20
d_l	15	C_F	300-2000
i_f	4		
C_E	5		
$i_{.e.,}$	4		
d	10		
i_m	5		
n_l	5		
n	10		

Procedure for Prediction of Economic Performance

The procedure for calculating the absorbed irradiation and the heat losses for conventional flat plate SAH is used. Further, by knowing the thermal performance, economic evaluation is being done, i.e., life cycle savings are calculated.

If the system requires a total investment 'C' of which a fraction f_l is taken as a loan amount, then loan taken, and down payment are given as:

$$Loan\ taken = f_l C$$

$$Down\ payment = (1 - f_l)C$$

Assuming the interest rate on loan to be d_l and that it is to be paid back in equal annual instalments over a period of n_l years. For any year j, the annual repayment on loan is given as:

(6) $$Annual\ repayment\ on\ loan = \frac{d_l(f_l C)}{\left[1 - \left\{\frac{1}{(1+d_l)^{n_l}}\right\}\right]}$$

The collector cost is determined from the conventional collector cost factor C_C, which is the unit area cost of smooth surface. In this, the cost of roughness configurations fixed to the absorber plate is also added. If C_R is the roughness cost factor that represents material cost and the fabrication cost per unit cubic meters of roughness material per unit area of the collector plate.

Then,

(7) $$C = A_P(C_C + C_R V_R)$$

where, $A_P = W \times L$

where w and L are width and length of the absorber plate.

(8) $$V_R = \frac{\pi D_h \left(\frac{e}{D_h}\right)}{4\left(\frac{p}{e}\right) Sin\left(\frac{\alpha}{2}\right)}$$

(9) $$D_h = \frac{2 \times W \times H}{(W + H)}$$

V_R is the volume of the material attached as roughness to absorber plate in cubic metres per meter square of collector plate area, D_h is hydraulic diameter of the solar air heater duct.
The annual savings of conventional fuel is converted into money by multiplying it with the cost factor of conventional fuel (C_F), which is the unit cost of conventional fuel, which increases at the rate of i_f per year and is then calculated for j^{th} year as:

(10) $$Fuel\ Savings = C_F E\left(1 + i_f\right)^{(j-1)}$$

where E is the annual solar energy collected.
The cost of maintenance is taken as M in the first year of operation, and that it increases at the rate of i_m every year, the maintenance cost for the j^{th} year is given as:

(11) $$Maintenance\ cost = M(1 + i_m)^{(j-1)}$$

This pumping energy (E_P) for the running of a pump to continuously flow air in solar collector comes from the electricity. So, the electricity bill over a year of this pumping energy is calculated by multiplying the cost factor of electricity (C_E) by the pumping energy. Let this cost of electricity increases at the rate of i_e per year. So, the electricity bill for running the pump in j^{th} year is given as:

(12) $$Electricity\ Bill = C_E E_P (1 + i_e)^{(j-1)}$$

Neglecting the tax deduction on the interest component of loan repayment and tax deduction on depreciation, the annual solar savings (*ASS*) in the j^{th} year is given as:

(13) $$ASS = C_F E\left(1 + i_f\right)^{(j-1)} - \frac{d_l(f_l C)}{\left[1 - \left\{\frac{1}{(1 + d_l)^{n_l}}\right\}\right]} - M(1 + i_m)^{(j-1)} - C_E E_P (1 + i_e)^{(j-1)}$$

This equation is valid for $j \leq n_l$.

The *LCS* over a period of *n* years for the system is obtained by summing up the present worth of the annual solar savings and considering initial down payment. Thus, *LCS* is given by:

(14) $$LCS = \sum_{j=1}^{n} (ASS)_j - (Initial\ down\ payment)$$

Taking market discount rate as '*d*', and *ASS* from Eq. 13, we obtain *LCS* as given in Eq. 15.

The Eq. (15) is valid for $n \geq n_l$, $d \neq i_f$, $d \neq i_m$, and $d \neq i_f$.

$$LCS = -(1-f_l)C + \frac{C_F E}{(d-i_f)}\left\{1-\left(\frac{1+i_f}{1+d}\right)^n\right\} - \frac{d_l(f_l C)}{\left[1-\left\{\frac{1}{(1+d_l)^{n_l}}\right\}\right]}\frac{1}{d}\left\{1-\frac{1}{(1+d)^{n_l}}\right\} - \frac{M}{(d-i_m)}\left\{1-\left(\frac{1+i_m}{1+d}\right)^n\right\} - \frac{C_E E_P}{(d-i_e)}\left\{1-\left(\frac{1+i_e}{1+d}\right)^n\right\} \quad (15)$$

Results and Discussions

The results obtained from the mathematical simulation to evaluate the economic performance viz. *LCS* of a solar thermal collector have been reported and discussed in this section.

Life Cycle Savings

Figure 2 reveals that the values of *LCS* are negative for some years in each case, although this number depends on the values of the *ΔT/I*, a lower value of this parameter requires a longer period for the *LCS* to become positive because of higher electricity bill due to high mass flow rate. Thus, larger pumping power is required even if it possess a relatively higher thermal efficiency. The maximum *LCS* are seen in this plot for the *ΔT/I* of 0.010 and then with an increase in *ΔT/I*, LCS decreases. This is due to low Q_u for the higher values of *ΔT/I* which in turn reduces fuel savings and yields lower values of *LCS*.

From Figures 3 and 4 it is seen that the cost factor of collector has a significant impact on *LCS*, a lower value of collector cost of Rs. 1000/m^2 results in a breakeven (*LCS* equal to zero) in less than 3 years, whereas if the cost of collector is 20 times (Figure 4), the breakeven is reached much later (in almost 9 years).

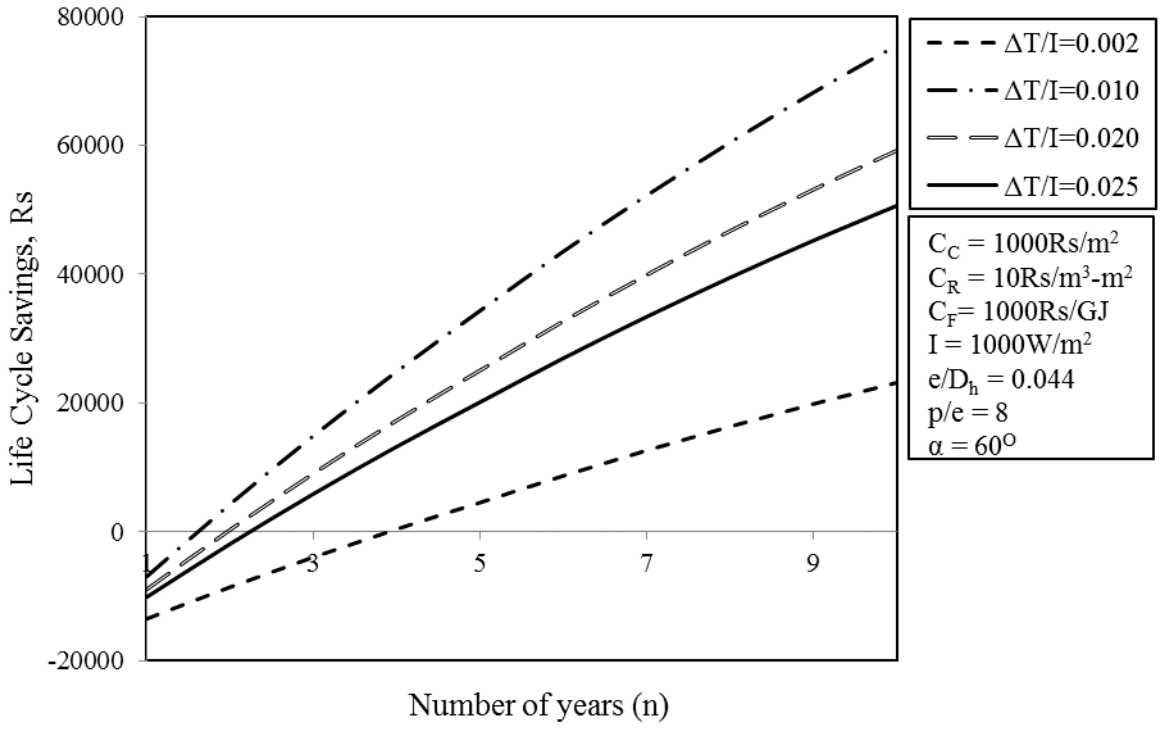

Figure 2. Variation of LCS with number of years for different ΔT/I.

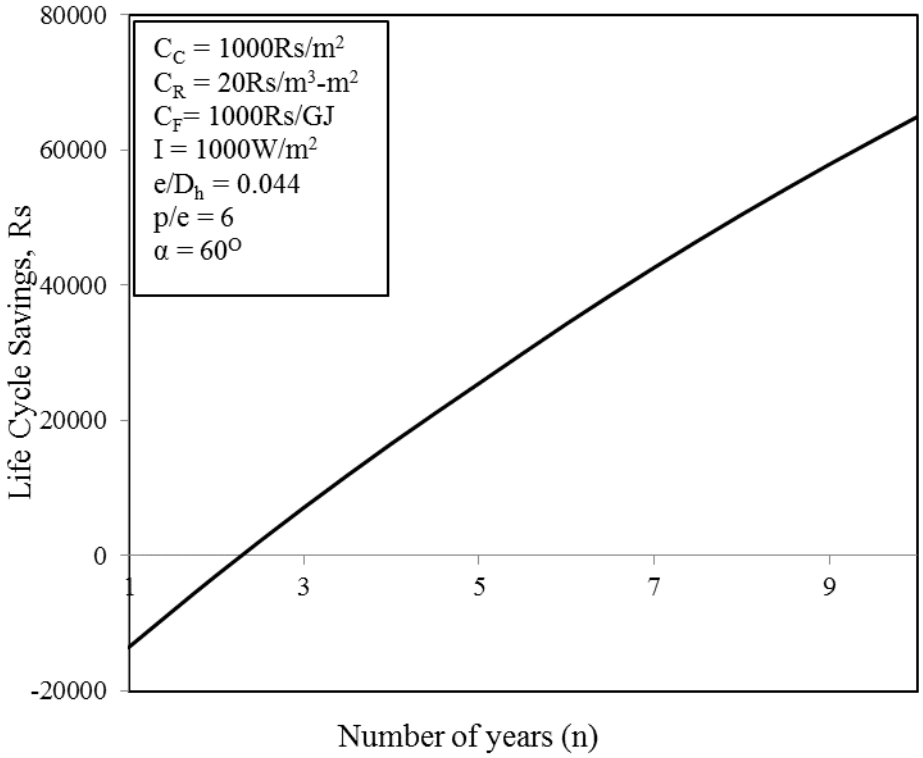

Figure 3. Variation of *LCS* with number of years with C_C as 1000Rs/m^2.

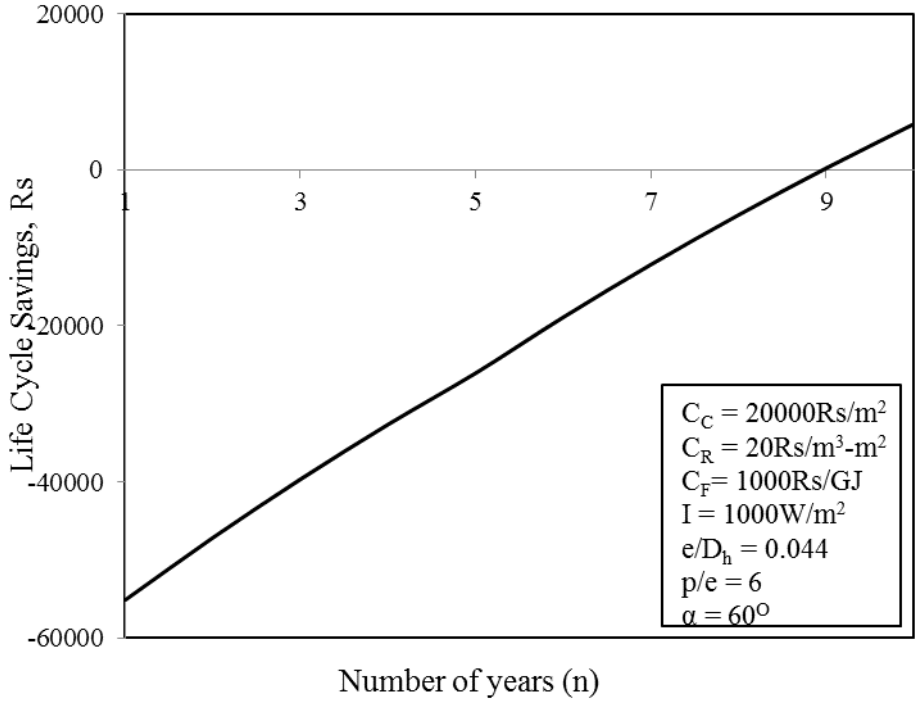

Figure 4. Variation of *LCS* with number of years with C_C as 20000Rs/m^2.

Effect of Cost Factor of Collector on LCS

It can be seen clearly from the Figures 5 and 6 that *LCS* value decreases sharply with the increase in C_C. Further, a very large value may even result in a negative value. It can also be seen that *LCS* increase as the values of $\Delta T/I$ raises, and after attaining maximum value, *LCS* declines with further increase of $\Delta T/I$. Very low values of $\Delta T/I$ are accompanied with significantly large values of pumping power. Furthermore, high thermal efficiencies accumulated cannot compensate the high electricity bill of pumping power. While higher values of $\Delta T/I$ results

in lower thermal efficiency and hence lower fuel savings leading to lower values of *LCS* as can be seen from Figure 5. Figure 6 has been plotted to reveal the above-mentioned results more clearly where an increase in C_C values always results in lower values of *LCS*, a linear variation for any fixed value of $\Delta T/I$ is seen.

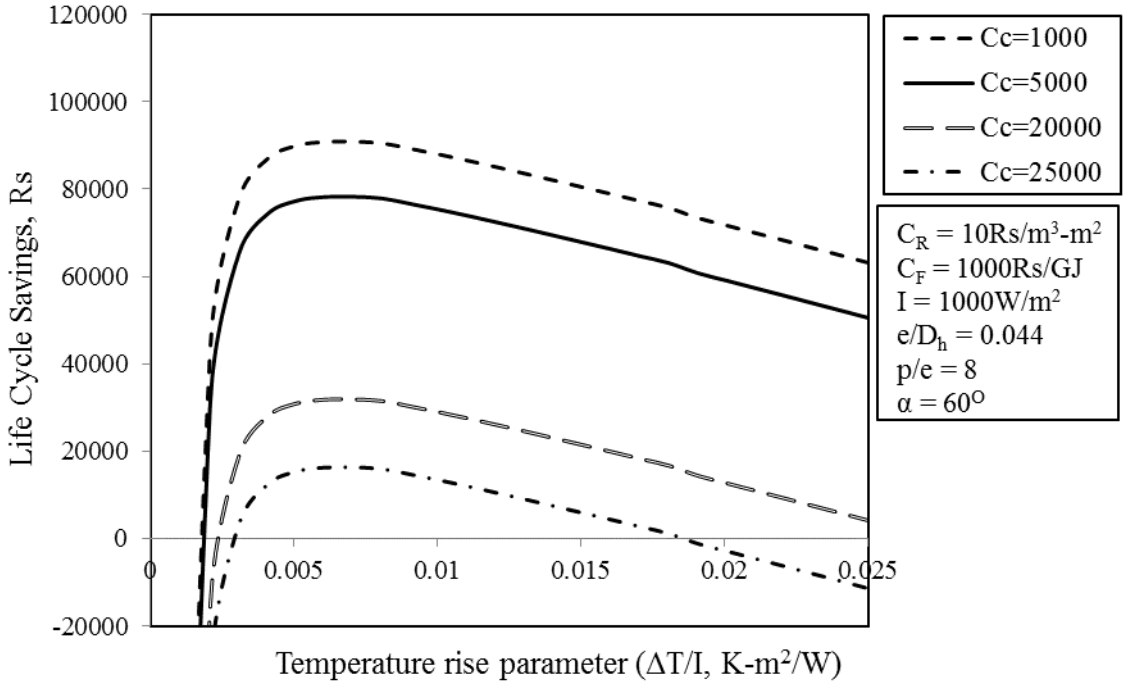

Figure 5. Variation of *LCS* with $\Delta T/I$ with different C_C.

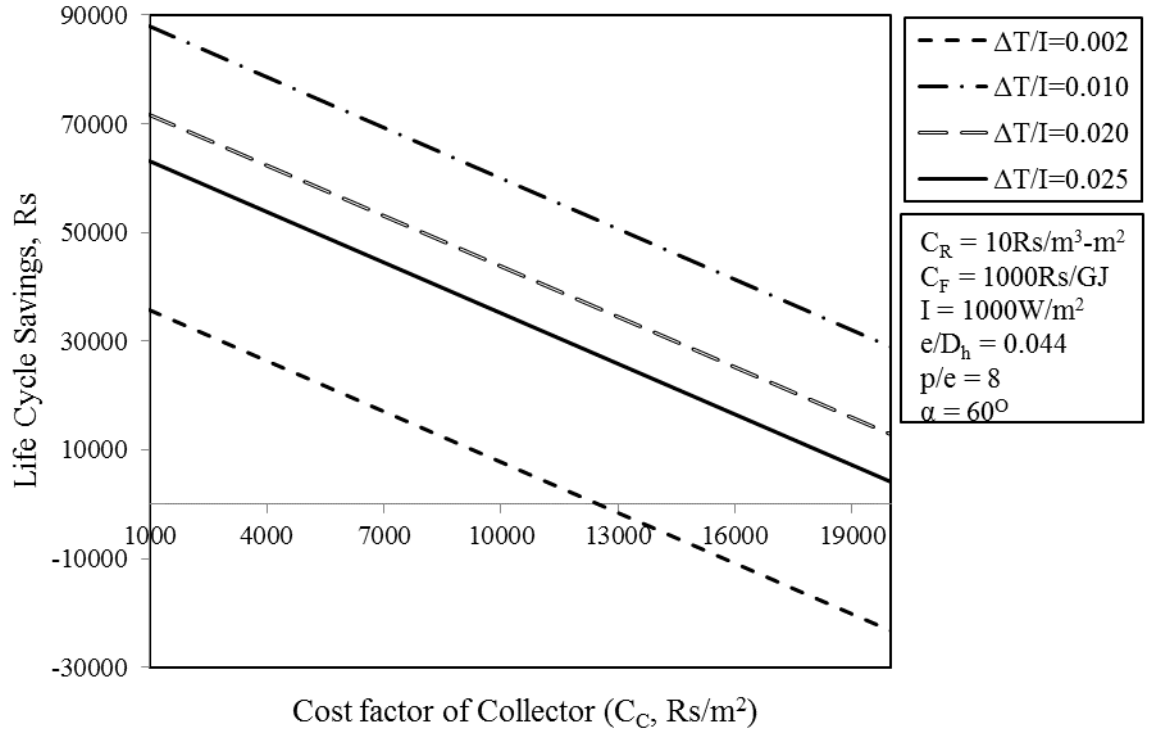

Figure 6. Variation of *LCS* with C_C with different $\Delta T/I$.

Effect of Artificial Roughness Parameters on LCS

From Figure 7, it is to be noted that as the e/D_h of the roughness elements increases, *LCS* decreases in the case of lower values of $\Delta T/I$, whereas for the higher values of $\Delta T/I$, the *LCS* increases. It is also seen that there is no single optimum value of roughness height for the entire range of temperature rise parameter that would give the maximum value of *LCS*. In Fig. 8 the values of *LCS* are presented for various e/D_h values, where it is revealed

that functional changes depend on *ΔT/I*; a lower value of *ΔT/I* show a decrease in the value of *LCS* as roughness height is increased from a value of 0.020 to 0.044 indicating best value of 0.020, whereas corresponding to higher *ΔT/I* value of 0.025, the best value is 0.044 (that corresponds to maxima in *LCS*). The fact that lower *ΔT/I* correspond to higher electric power expenses involved with pumping power as well as the cost of roughness components explains the difference in the optimal values. Whereas, corresponding to higher *ΔT/I*, the Q_u and the resultant conventional fuel cost savings are likely to predominate.

Plots showing the effects of *p/e* of roughness elements on *LCS* are presented in Figures 9 and 10. Where for lower values of *ΔT/I*, *LCS* obtains maximum value corresponding to *p/e* of 12. Further, for *ΔT/I* > 0.008 the utmost value of *LCS* is found for *p/e* value of 10. These results have been replotted in Figure 10 where variation of *LCS* with *p/e* is shown for different values of *ΔT/I* and it is revealed that the values of LCS increases first with increase in *ΔT/I* and after obtaining maxima at *ΔT/I* value of 0.010 it starts declining; for *ΔT/I* value of 0.010, highest *LCS* is obtained for *p/e* value of 12.

The effect of *α* on *LCS* are presented in Figures 11 and 12. Where Figure 11 shows that the maximum values of *LCS* correspond to lowest value of *α* of 30° for lower *ΔT/I* whereas the highest value of *α* of 75° correspond to maxima in *LCS* when *ΔT/I* values are high. These results are again shown in different manner where variation of *LCS* with *α* are shown for different values of *ΔT/I* and it is revealed that maximum LCS is obtained for *ΔT/I* value of 0.010. Also, the values of LCS first increases with *ΔT/I* and after attaining maxima, it starts decreases. For the maximum value of LCS obtained for *ΔT/I*=0.010*, the α* value is 75°.

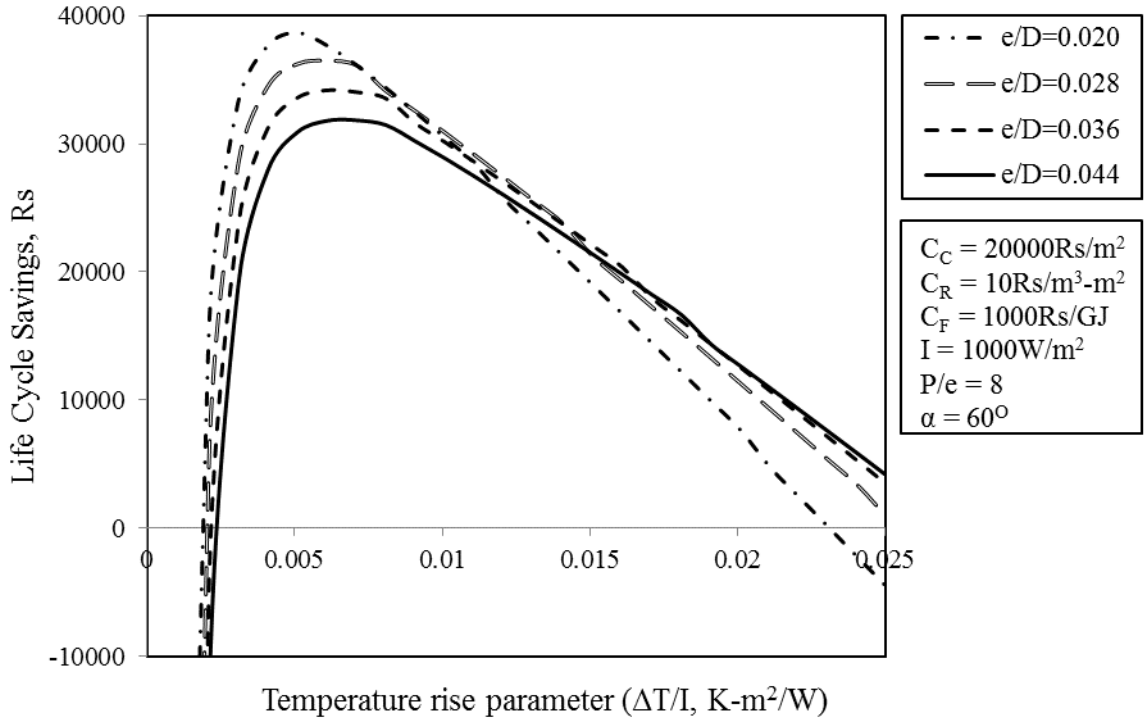

Figure 7. Variation of *LCS* with *ΔT/I* for different e/D_h.

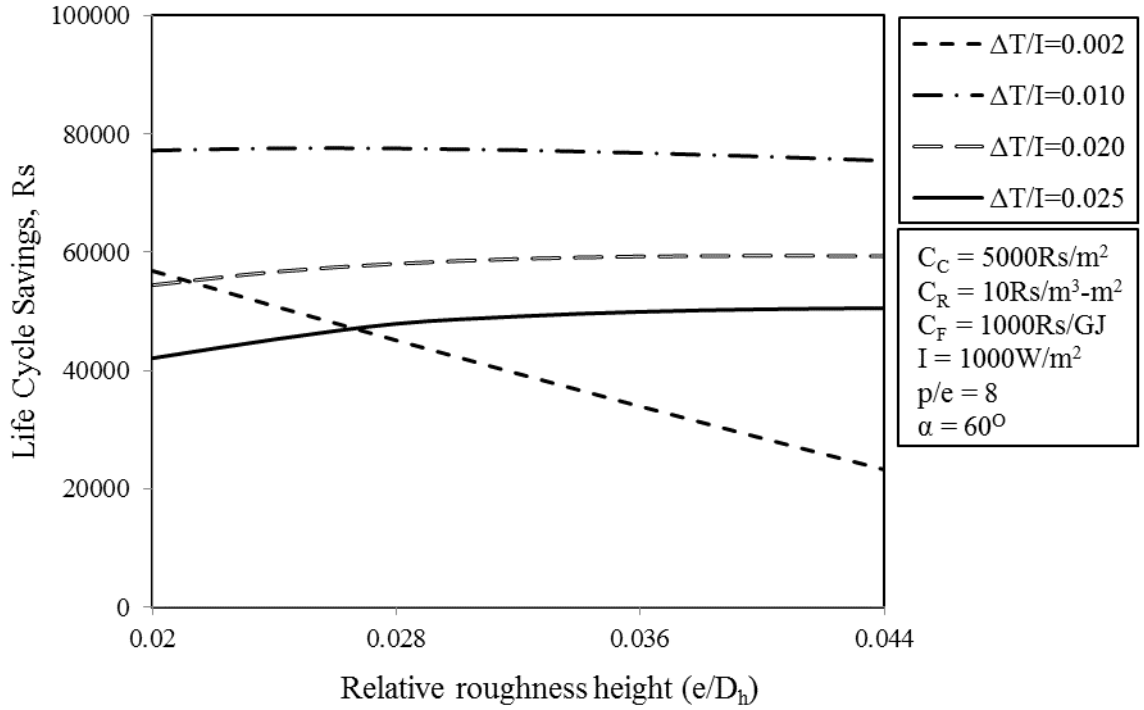

Figure 8. Variation of *LCS* with e/D_h for different $\Delta T/I$.

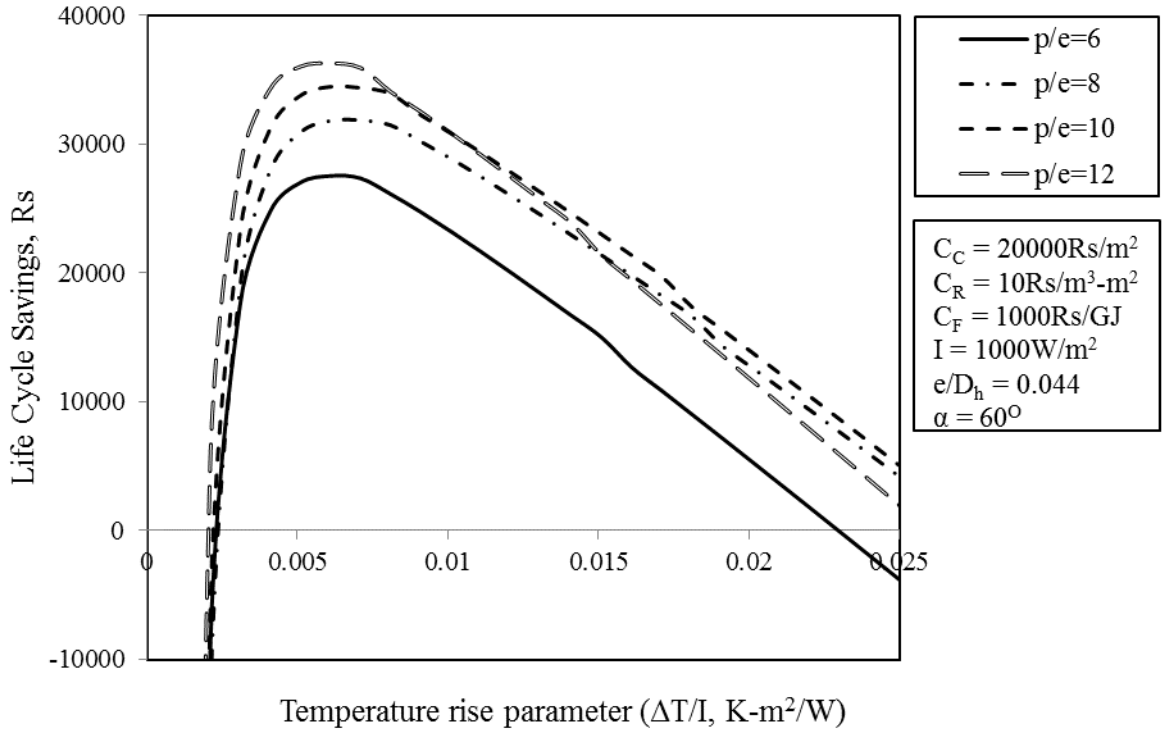

Figure 9. Variation of *LCS* with $\Delta T/I$ for different *p/e*.

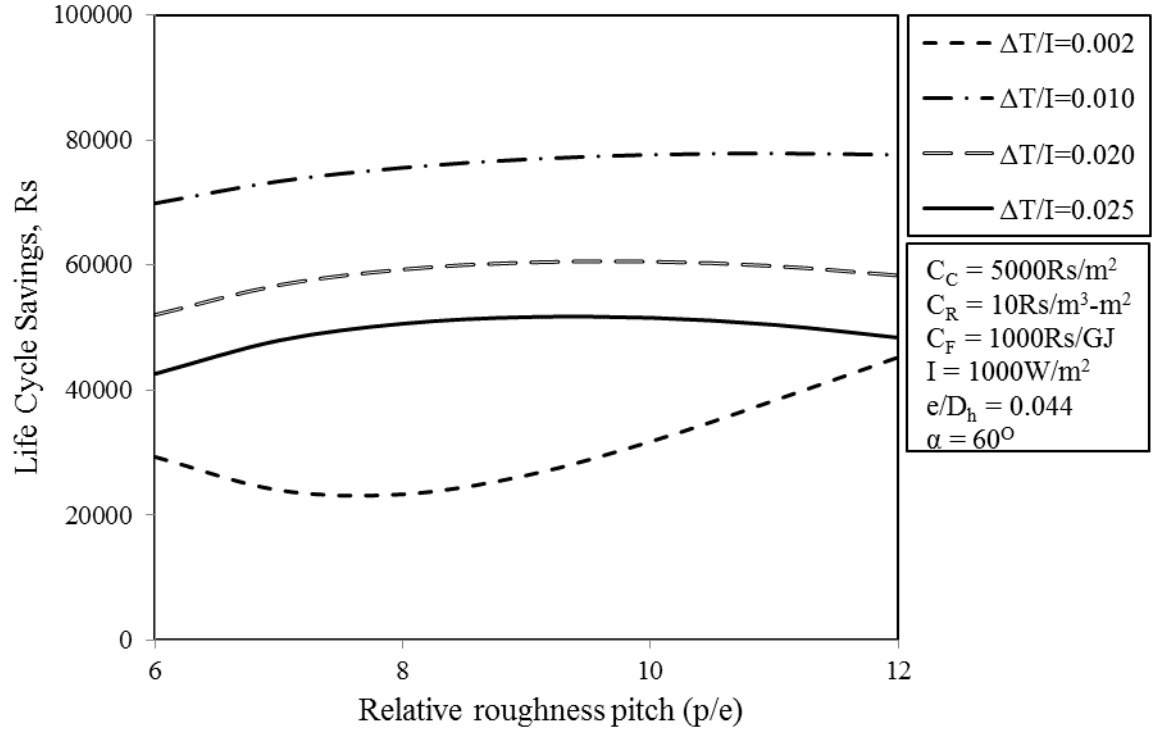

Figure 10. Variation of *LCS* with *p/e* for different *ΔT/I.*

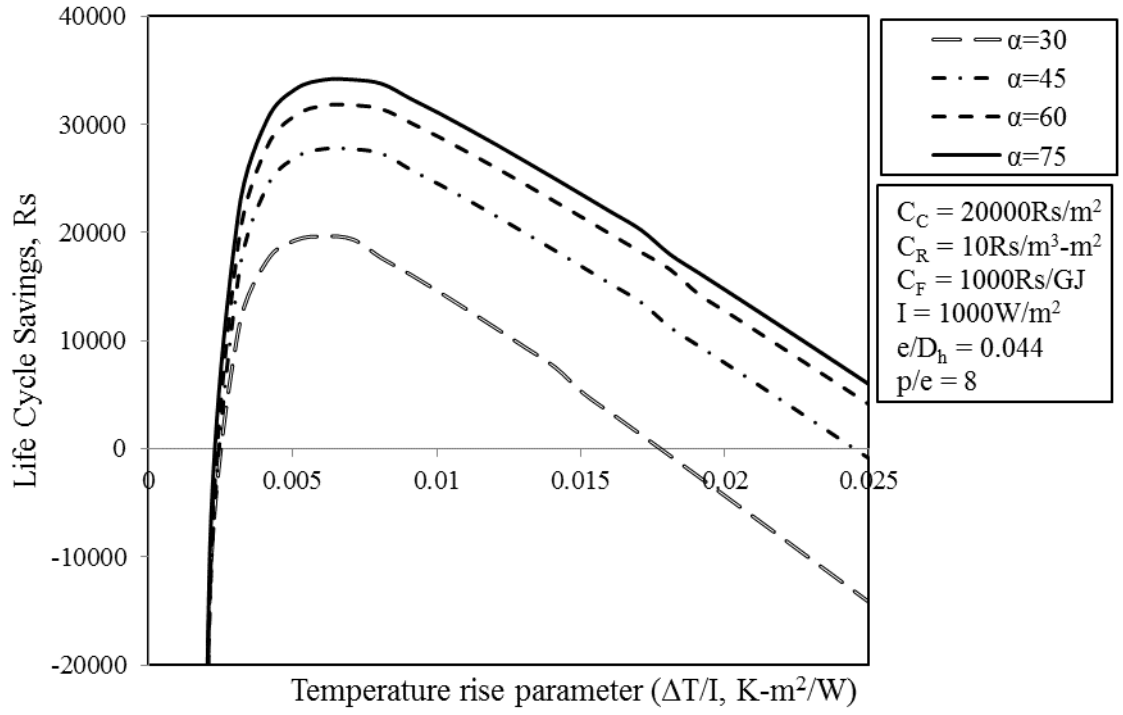

Figure 11. Variation of *LCS* with *ΔT/I* for different *α.*

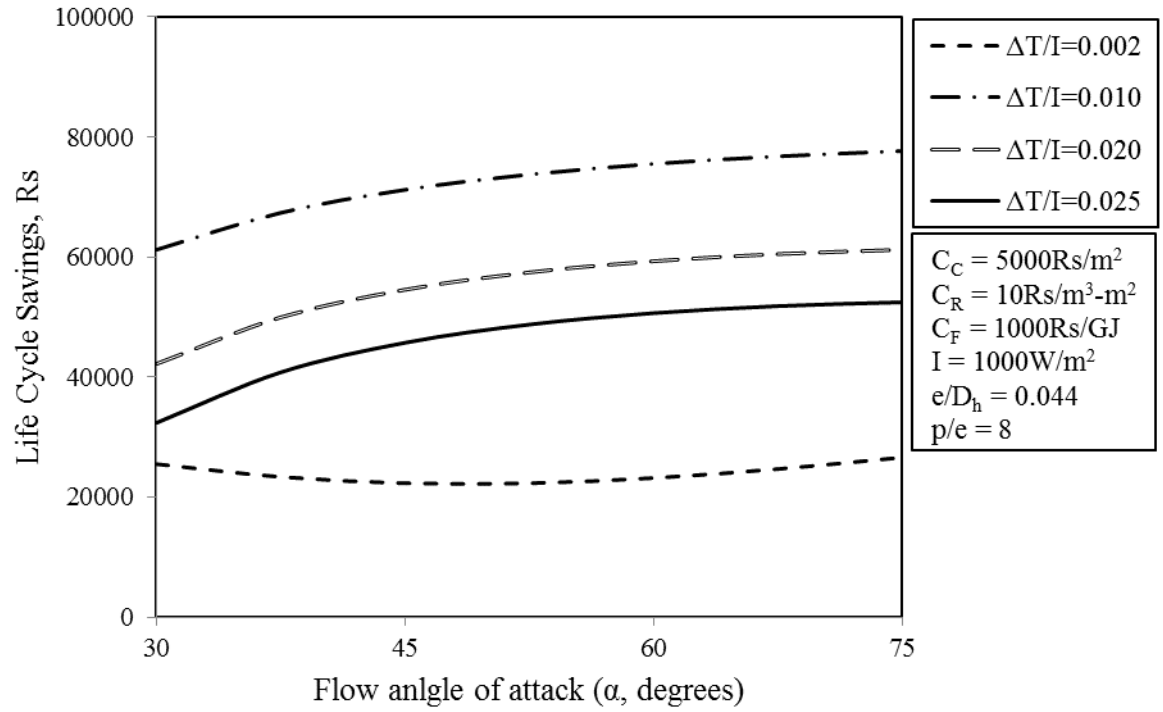

Figure 12. Variation of *LCS* with *α* for different *ΔT/I*.

Effect of Roughness Cost Factor on LCS

Higher cost of material and fabrication per unit volume of material results in substantially lower values of *LCS* and the results can be seen from Figures 13 and 14. It is thus evident that roughness elements cost are added to the collector cost, but these are function of roughness parameters too. The maximum *LCS* is obtained for the lowest value of C_R of 2, and as C_R increases from 2 to 20, the values of *LCS* decreases. Another interesting outcome of variation of *LCS* with C_R is seen in Figure 14, where it is evident that the *LCS* has a linear variation with values of C_R for a particular value of *ΔT/I*. this is mainly since as C_R increases the cost of the collector increases thereby increasing the initial investment costs, which in turn decreases the *LCS*.

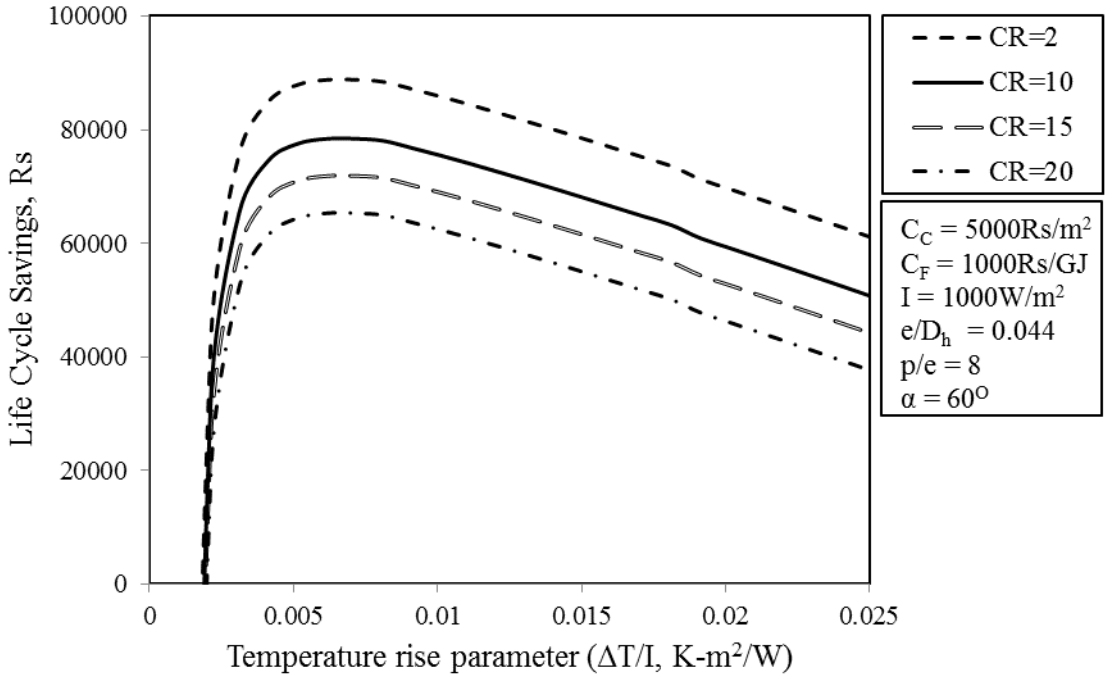

Figure 13. Variation of *LCS* with *ΔT/I* for different C_R.

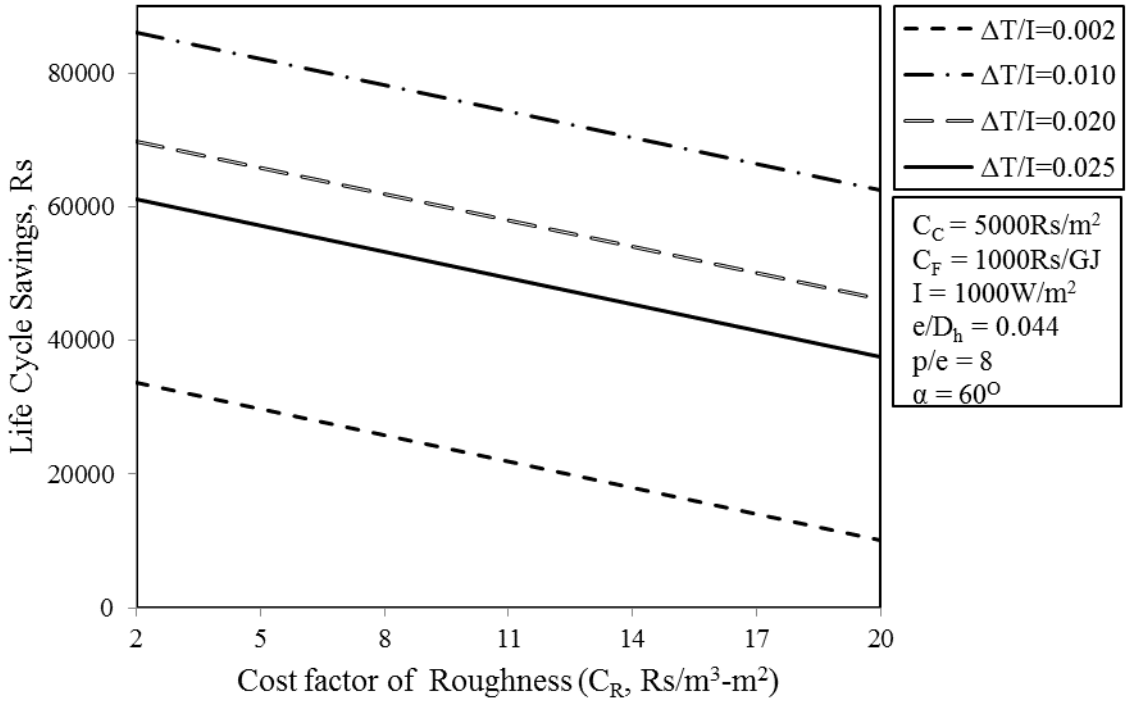

Figure 14. Variation of *LCS* with C_R with different *ΔT/I.*

Effect of Cost Factor of Conventional Fuel on LCS

To study the effect of C_F on *LCS*, plots of *LCS* for different values of the C_F are presented in Figures 15 and 16. It is clearly seen that the *LCS* is a strong function of C_F and it increases substantially with an increase in C_F. Maximum *LCS* is found for maximum value of C_F of 2000. This is attributed to the fact that as CF increases from 300 to 2000, the solar fuel savings increases, because for same amount of energy saved by solar energy, the cost of energy is high if that same amount of energy is utilized by convention fuel of high cost as compared to convention fuel of low cost. Hence higher values of C_F give better *LCS*. Also, from Figure 16, it is seen that the variation of LCS with CF is linear for a particular value of *ΔT/I.*

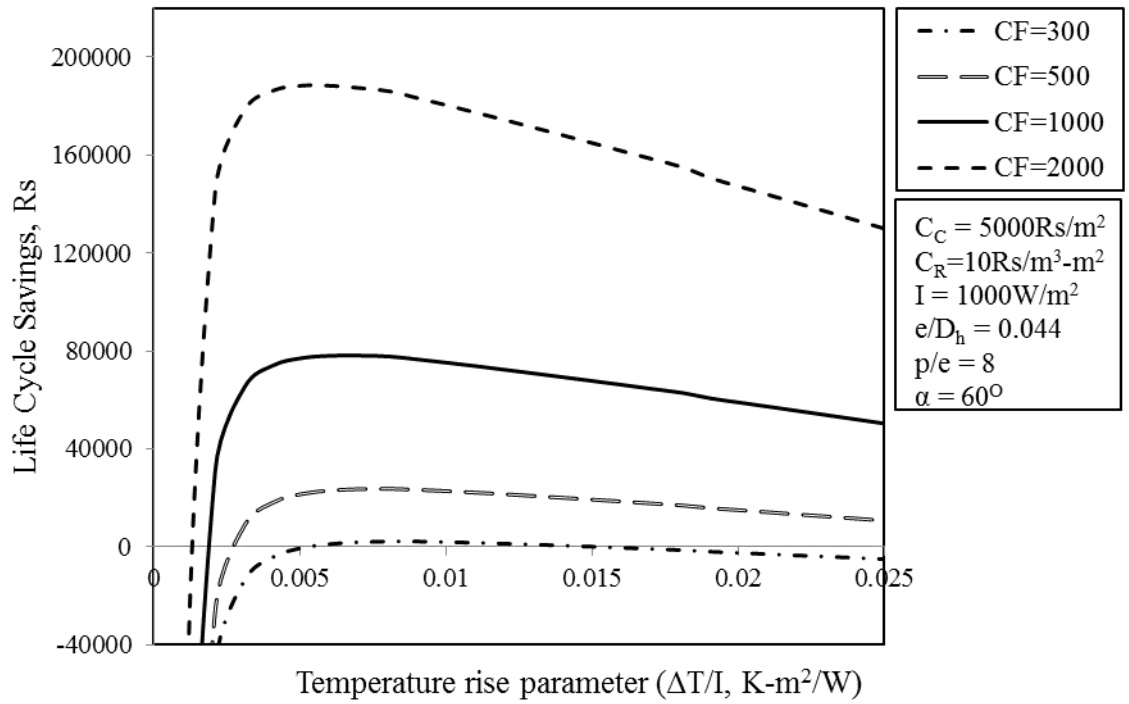

Figure 15. Variation of *LCS* with *ΔT/I* for different C_F.

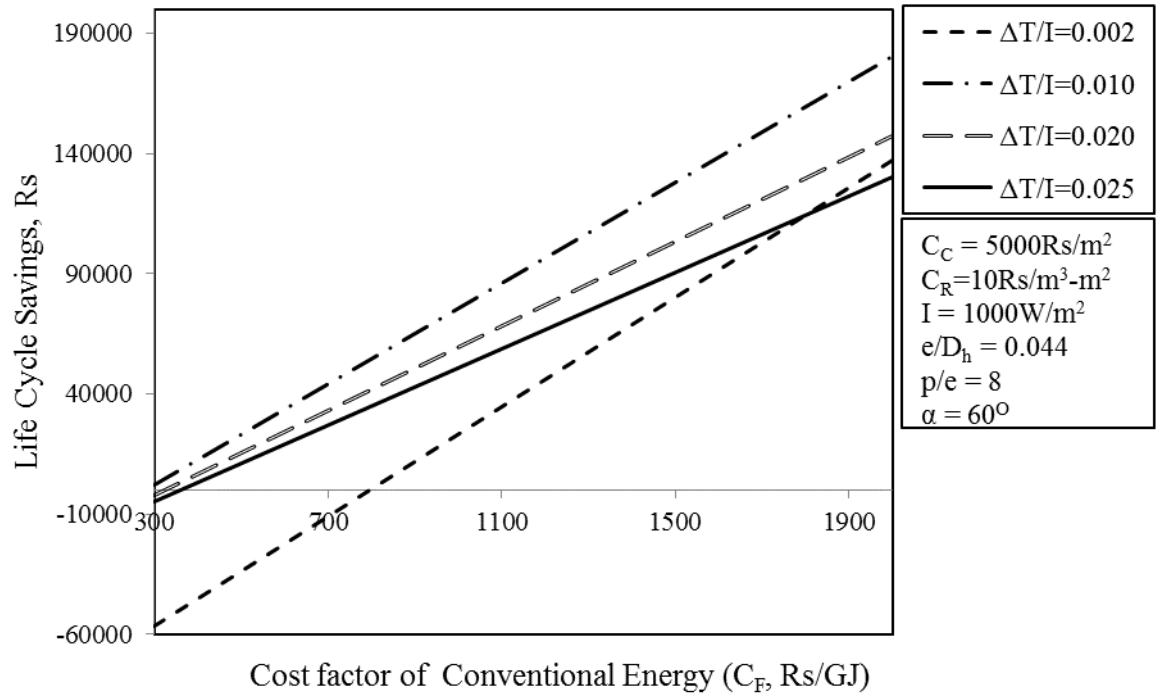

Figure 16. Variation of *LCS* with C_F with different *ΔT/I*.

Impact

The usage of solar air heaters in residential and commercial applications to replace traditional heaters is growing, garnering the attention of numerous investigators who are working to improve the efficiency of solar air heaters while lowering their installation and operating costs.

In the recent times, due to the increased cost of non-renewable energy resources, the financial aspect of using solar air heater has become more prominent. The investors will consider investing in solar air heater only if it is profitable in comparison to conventional air heaters, hence it is imperative to assess the economic viability of solar air heater before installing it for industrial and domestic use. The present research work deals exactly with this problem and gives designers the complete economic analysis of an artificially roughened solar air heater with v-shaped ribs for different system and variable parameters.

From the results of economic analysis, it can be stated that there exists a set of optimum values of roughness parameters which maximizes the life cycle savings of a SAH, and this set of parameters comprising of e/D_h, p/e, and α, is a strong function of operating parameters namely $\Delta T/I$ and I and the economic parameters, namely C_C, C_R and C_F. For lower values of $\Delta T/I$ the 0.020 value e/D_h, 12 value of p/e and 30° of α gives highest values of *LCS*. Whereas for higher values of $\Delta T/I$ the 0.044 value e/D_h, 10 value of p/e and 75° of α gives highest values of *LCS*. Also, the best values of C_C, C_R and C_F for which maximum *LCS* is obtained are 1000, 2, and 300 respectively.

Moreover, through this research, the designers now have a vast data of economic analysis for different system and variable parameters of solar air heater with v-shaped ribs, which is very scarce in this field. Hence the use of solar air heater is expected to increase after this research work thereby increasing the share of solar energy in the global energy mix and reducing carbon emission from conventional fuel combustion for air/space heating; also facilitating the saving of natural resources.

It should also be noted that the installation of a solar air heater, which will be used for drying or space heating, assumes the availability of appropriately qualified personnel, which will result in the creation of new jobs, the number of which depends on the scale of implementation, thus producing socio-economic impact too in the society.

Conclusions

Based on this work, the following conclusions have been drawn:

1. There is a strong effect of roughness parameters on *LCS* of an artificially roughened SAH. Maximum values of *LCS* obtained corresponds to the lowest value of e/D_h in the case of $\Delta T/I < 0.007$, whereas for $\Delta T/I > 0.007$ highest values of *LCS* is found for highest values of e/D_h.

2. The utmost *LCS* comes at *p/e* value of 12 for lower values of *ΔT/I* (less than 0.008), while the max *LCS* comes at a *p/e* value of 10 for larger values of *ΔT/I* (greater than 0.008).
3. C_C as well as C_R plays an important role in determining the *LCS* of an artificially roughened SAH. An increase in C_C and C_R values results in a substantially large decrease in *LCS.* Further, an increase of collector cost, as well as roughness cost beyond a certain limit, may result in negative *LCS*.
4. C_F is another promising parameter on which *LCS* of an artificially roughened SAH depends. With an increase in C_F, *LCS* increases.

Conflict of Interest

There are no conflicts to declare.

Acknowledgements

This research has not been supported by any external funding.

References

[1] K. Prasad, S.C. Mullick, Heat transfer characteristics of a solar air heater used for drying purposes, Appl. Energy. 13 (1983) 83–93. https://doi.org/10.1016/0306-2619(83)90001-6.

[2] A.M. Ebrahim Momin, J.S. Saini, S.C. Solanki, Heat transfer and friction in solar air heater duct with V-shaped rib roughness on absorber plate, Int. J. Heat Mass Transf. 45 (2002) 3383–3396. https://doi.org/10.1016/S0017-9310(02)00046-7.

[3] V.S. Hans, R.P. Saini, J.S. Saini, Heat transfer and friction factor correlations for a solar air heater duct roughened artificially with multiple v-ribs, Sol. Energy. 84 (2010) 898–911. https://doi.org/10.1016/j.solener.2010.02.004.

[4] S. Chamoli, N.S. Thakur, Heat transfer enhancement in solar air heater with V-shaped perforated baffles, J. Renew. Sustain. Energy. 5 (2013) 023122. https://doi.org/10.1063/1.4798411.

[5] V.B. Gawande, A.S. Dhoble, D.B. Zodpe, S. Chamoli, Experimental and CFD-based thermal performance prediction of solar air heater provided with chamfered square rib as artificial roughness, J. Brazilian Soc. Mech. Sci. Eng. 38 (2016) 643–663. https://doi.org/10.1007/s40430-015-0402-9.

[6] R. Maithani, J.S. Saini, Heat transfer and friction factor correlations for a solar air heater duct roughened artificially with V-ribs with symmetrical gaps, Exp. Therm. Fluid Sci. 70 (2016) 220–227. https://doi.org/10.1016/j.expthermflusci.2015.09.010.

[7] R. Nadda, A. Kumar, R. Maithani, Developing heat transfer and friction loss in an impingement jets solar air heater with multiple arc protrusion obstacles, Sol. Energy. 158 (2017) 117–131. https://doi.org/10.1016/j.solener.2017.09.042.

[8] V. Singh Bisht, A. Kumar Patil, A. Gupta, Review and performance evaluation of roughened solar air heaters, Renew. Sustain. Energy Rev. 81 (2018) 954–977. https://doi.org/10.1016/j.rser.2017.08.036.

[9] I. Singh, S. Singh, CFD analysis of solar air heater duct having square wave profiled transverse ribs as roughness elements, Sol. Energy. 162 (2018) 442–453. https://doi.org/10.1016/j.solener.2018.01.019.

[10] S. Chamoli, R. Lu, D. Xu, P. Yu, Thermal performance improvement of a solar air heater fitted with winglet vortex generators, Sol. Energy. 159 (2018) 966–983. https://doi.org/10.1016/j.solener.2017.11.046.

[11] R. Maithani, A. Kumar, P. Gholamali Zadeh, M.R. Safaei, E. Gholamalizadeh, Empirical correlations development for heat transfer and friction factor of a solar rectangular air passage with spherical-shaped turbulence promoters, J. Therm. Anal. Calorim. 139 (2020) 1195–1212. https://doi.org/10.1007/s10973-019-08551-8.

[12] R. Bahuguna, K.K.S. Mer, M. Kumar, S. Chamoli, Thermohydraulic performance and second law analysis of a tube embedded with multiple helical tape inserts, Energy Sources, Part A Recover. Util. Environ. Eff. (2021) 1–23. https://doi.org/10.1080/15567036.2021.1904057.

[13] S. Paneliya, S. Khanna, V. Mankad, A. Ray, P. Prajapati, I. Mukhopadhyay, Comparative study of heat transfer characteristics of a tube equipped with X-shaped and twisted tape insert, Mater. Today Proc. 28 (2019) 1175–1180. https://doi.org/10.1016/j.matpr.2020.01.103.

[14] R. Bahuguna, K.K.S. Mer, M. Kumar, S. Chamoli, Entropy generation analysis in a tube heat exchanger integrated with triple blade vortex generator inserts, Energy Sources, Part A Recover. Util. Environ. Eff. (2021) 1–19. https://doi.org/10.1080/15567036.2021.1918291.

[15] R. Kumar, P. Chandra, Thermal analysis, pressure drop and exergy loss of energy efficient shell, and triple meshed helical coil tube heat exchanger, Energy Sources, Part A Recover. Util. Environ. Eff. 42 (2020) 1026–1039. https://doi.org/10.1080/15567036.2019.1602213.

[16] V.S. Bisht, A.K. Patil, A. Gupta, Thermo-Hydraulic Performance of Solar Air Heater Roughened with V- haped Ribs Combined with V-Shaped Perforated Baffles, Adv. Energy Res. 2 (2020) 123–132. https://doi.org/10.1007/978-981-15-2662-6_12.

[17] H.U. Choi, K.H. Choi, CFD analysis on the heat transfer and fluid flow of solar air heater having transverse triangular block at the bottom of air Duct, Energies. 13 (2020) 1099. https://doi.org/10.3390/en13051099.

[18] H.K. Ghritlahre, P.K. Sahu, A comprehensive review on energy and exergy analysis of solar air heaters, Arch. Thermodyn. 41 (2020) 183–222. https://doi.org/10.24425/ather.2020.134577.

[19] H. Singh, H. Singh, R. Bahuguna, C. Kishore, CFD analysis of heat transfer characteristics of rectangular solar air heater with kite shaped roughness, Mater. Today Proc. 52 (2022) 2014–2025. https://doi.org/10.1016/j.matpr.2021.12.008.

[20] L.N. Azadani, N. Gharouni, Multi objective optimization of cylindrical shape roughness parameters in a solar air heater, Renew. Energy. 179 (2021) 1156–1168. https://doi.org/10.1016/j.renene.2021.07.084.

[21] A. Haldar, L. Varshney, P. Verma, Effect of roughness parameters on performance of solar air heater having artificial wavy roughness using CFD, Renew. Energy. 184 (2022) 266–279. https://doi.org/10.1016/j.renene.2021.11.088.

[22] A. Malhotra, H.P. Garg, A. Patil, Heat loss calculation of flat plate solar collectors, J. Therm. Eng. 2 (1981) 59–62.